Copy 6
RM L53H20

NACA RM L53H20

RESEARCH MEMORANDUM

TRANSONIC FLIGHT TESTS TO DETERMINE ZERO-LIFT DRAG AND PRESSURE RECOVERY OF NACELLES LOCATED AT THE WING ROOT ON A 45° SWEPTBACK WING AND BODY CONFIGURATION

By Sherwood Hoffman and Austin L. Wolff

Langley Aeronautical Laboratory
Langley Field, Va.

NATIONAL ADVISORY COMMITTEE
FOR AERONAUTICS

WASHINGTON
September 29, 1953

NACA RM L53H20

NATIONAL ADVISORY COMMITTEE FOR AERONAUTICS

RESEARCH MEMORANDUM

TRANSONIC FLIGHT TESTS TO DETERMINE ZERO-LIFT DRAG AND PRESSURE RECOVERY OF NACELLES LOCATED AT THE WING ROOT ON A 45° SWEPTBACK WING AND BODY CONFIGURATION

By Sherwood Hoffman and Austin L. Wolff

SUMMARY

The zero-lift drag of a sweptback wing and body configuration with nacelles was determined by flight tests of rocket-propelled models at Mach numbers from 0.8 to 1.3. Tests were made of solid and ducted nacelles located at the wing root and were compared with previous tests of the nacelles at the wing tip. Ground tests were made of a ducted nacelle to calibrate the flow in the duct at supersonic speeds. The wing had a sweepback angle of 45° along the quarter-chord line, an aspect ratio of 6.0, a taper ratio of 0.6, and an NACA 65A009 airfoil section in the free-stream direction. The fuselage fineness ratio was 10.0. The solid and ducted nacelles had fineness ratios of 9.66 and 8.73, respectively.

The nacelle-plus-interference drag rise was in general dependent on the nacelle location and in part dependent on the resulting rate of development of cross-sectional area of the aircraft configuration. Little or no unfavorable interference effects were obtained from the inboard nacelles above Mach number 1.05 and below Mach number 0.93, whereas, favorable interference was obtained from the wing-tip nacelles throughout the speed range. The wing and body had a negligible effect on the total-pressure recovery of the inlet diffuser in either the inboard or wing-tip nacelle positions. The total-pressure recovery from the nacelles was 98 percent at a mass-flow ratio of about 0.7 throughout the flight range. The drag-rise Mach number of the configuration with inboard nacelles was 0.93, which was about 0.03 Mach number lower than that for the configuration with and without the wing-tip nacelles.

INTRODUCTION

As part of a general transonic research program of the National Advisory Committee for Aeronautics to investigate the aerodynamic properties of promising aircraft configurations, the Langley Pilotless Aircraft Research Division (at its testing station at Wallops Island, Va.) has tested several rocket-propelled free-flight models to determine the variations of zero-lift drag coefficient with Mach number for a high-aspect-ratio-wing—body configuration with nacelles located at various positions on the wing. The preliminary tests were conducted without air flow in the nacelles on the premise that the variations of nacelle-plus-interference drag coefficient with Mach number would be the same for the solid and ducted nacelles. This premise was supported by tests of solid and ducted nacelles located at the wing tips of the configuration (ref. 1). Drag data for the solid nacelles located in various spanwise, chordwise, and vertical positions on a 45° sweptback wing of aspect ratio 6.0 were published in references 1 to 7.

This investigation was undertaken to determine the aerodynamic properties of a nacelle located at the wing root of the basic configuration and to compare the nacelle properties with the results from an earlier investigation (ref. 1) of the nacelle tested at the wing tip. Data from tests of isolated nacelles obtained in this investigation and from reference 2 are also presented in order to determine the effects of interference on the nacelle drag and inlet pressure recovery.

The inlet of the nacelle consisted of an NACA 1-50-250 nose inlet with a critical Mach number above 0.9 and a conical subsonic diffuser that had a total angle of 7°. The nacelle was proportioned to house an axial-flow turbojet engine (about 50 inches in diameter, full scale) with an afterburner.

Because of the limited number of telemeter channels that could fit into the flight model, measurements of total-pressure recovery and static pressure were obtained from three total-pressure tubes and one static-pressure orifice located near the end of the diffuser. Preflight jet ground tests were made of an isolated nacelle (also reported in ref. 1) in order to calibrate the internal flow at Mach numbers of 1.22, 1.42, 1.75, and approximately 0.8.

The flight tests covered a continuous range of Mach number from 0.8 to 1.3, with corresponding Reynolds numbers, based on wing mean aerodynamic chord, varying from 4×10^6 to 8×10^6.

SYMBOLS

A	area in duct or cross-sectional area, sq ft
a	tangential acceleration, ft/sec^2
b	wing span, ft
C_D	total drag coefficient, based on wing plan-form area
C_{D_N}	nacelle-plus-interference drag coefficient, based on nacelle frontal area
c	wing chord, ft
g	acceleration due to gravity, 32.2 ft/sec^2
H	total pressure, lb/sq ft
$\overline{H}$	average total pressure, lb/sq ft
l	length, ft
M	Mach number
m	mass flow through duct, slugs/sec
m_o	mass flow through a stream tube of area equal to inlet area under free-stream conditions, slugs/sec
p	static pressure, lb/sq ft
q	dynamic pressure, lb/sq ft
R_e	Reynolds number, based on wing mean aerodynamic chord
r	local radius of duct, in.
r_{eq}	radius of equivalent body of revolution, ft
S	total wing plan-form area, sq ft
S_N	frontal area of one nacelle, sq ft
W	weight of model during deceleration, lb
θ	angle between flight path and horizontal, deg

γ ratio of specific heats

x station

y ordinate, or location of total-pressure tube measured from center line of duct

Subscripts:

o free stream

d measuring station in duct

i inlet

f fuselage

MODELS

Details and dimensions of the flight models and nacelles used in this investigation are given in figures 1 and 2 and tables I to V. The cross-sectional area distributions and equivalent bodies of revolution of the models tested and of the configuration with wing-tip nacelles from reference 1 are presented in figure 3. The amount of area subtracted from the ducted nacelles in figure 3 to compensate for the internal flow is equal to the stream tube area at the mass-flow ratio measured at Mach number 1.0. Photographs of the models are shown as figure 4.

Basic research configuration.- The wing-body-fin combination was similar to those investigated in references 1 to 7. The wing had a sweepback angle of 45° along the quarter-chord line, an aspect ratio of 6.0 (based on total wing plan-form area), a taper ratio of 0.6, and an NACA 65A009 airfoil section in the free-stream direction. The leading edge of the wing intersected the fuselage contour at the maximum-diameter station. The fuselage fineness ratio was 10.0 and the ratio of total wing plan-form area to fuselage frontal area was 16.0.

Nacelles.- A comparison between the solid nacelle and ducted nacelle is given in figures 2(a) and 2(b). Each nacelle was a body of revolution having an NACA 1-50-250 nose inlet, a cylindrical midsection, and an afterbody having the proportions of form 111 (ref. 1). The fineness ratios of the ducted nacelle and solid nacelle (including nose plug) were 8.73 and 9.66, respectively.

For the flight model, the center lines of the nacelles were located in the wing plane parallel to the free-stream direction at about 15 percent of the semispan (fig. 1). The nose of the ducted nacelle was located at 40.5 percent of the local wing chord in front of the wing leading edge. This chordwise location with respect to the wing maximum thickness was the same as that used for other spanwise nacelle locations in references 1, 3, 5, and 7. There was about a 0.35-inch gap between the lip of the nacelle and the fuselage surface for boundary-layer bypass.

The inlet of the nacelle duct (fig. 2(d)) consisted of a conical diffuser with a 0.03-inch lip radius, a total angle of 7°, and an area ratio (A_d/A_i) of 1.42:1. Three total-pressure tubes and one static-pressure orifice were located about 0.5 inch behind the diffuser. The total-pressure tubes were located at 0, 0.67, and 0.83 radius from the duct center line. The inner body of the nacelle, which was formed about that part of the wing passing through the duct, was a two-dimensional strut having a leading-edge radius of 0.335 inch and a thickness ratio of 8.4 percent (table III). The duct was contracted in the afterbody of the nacelle to have its minimum area at the exit. The exit area was approximately 82 percent of the inlet area.

The isolated nacelle used for the preflight jet tests (fig. 2(e)) was similar to the ducted nacelle on the flight model, except that the inner body in the cylindrical part of the nacelle was omitted. Four total-pressure tubes were mounted on a symmetrical circular-arc strut and located at 0, 0.42, 0.67, and 0.88 radius from the center line of the duct, as is shown in figure 2(e). The static-pressure orifice and total-pressure rake were located 0.5 inch behind the diffuser.

TESTS AND MEASUREMENTS

The flight tests and preflight jet ground tests were performed at the Langley Pilotless Aircraft Research Station at Wallops Island, Va.

During the tests the Reynolds number varied from approximately 4×10^6 at $M_0 = 0.8$ to 8×10^6 at $M_0 = 1.3$ for the flight tests and from about 4×10^6 at $M_0 \approx 0.8$ to 10.2×10^6 at $M_0 = 1.75$ for the preflight jet tests as is shown in figure 5.

Flight test.- Each flight model was propelled by a two-stage rocket system and launched from a rail launcher (fig. 4(a)). The first stage consisted of a 5-inch, lightweight, high-velocity aircraft rocket motor that served to accelerate the model from rest to high subsonic speeds. After burnout of the first stage, the booster separated from the model

and a 3.25-inch Mk 7 rocket motor installed in the fuselage (second stage) accelerated the model to supersonic speeds. The models were tracked by a CW Doppler velocimeter and an NACA modified SCR 584 tracking radar unit to determine the deceleration and trajectory during coasting flight. A survey of atmospheric conditions was made by radiosonde measurements from an ascending balloon that was released at the time of launching. A four-channel telemeter installed in the nose of the fuselage transmitted a continuous record of total-pressure and static-pressure measurements from one of the ducted nacelles to a ground receiving station.

The values of total drag coefficient, based on total-wing plan-form area, were calculated for decelerating flight by the relation

$$C_D = -\frac{W}{q_o g S}(a + g \sin \theta)$$

The nacelle-plus-interference drag coefficient was obtained from the differences in drag between a model without nacelles and a model with nacelles. This coefficient, based on nacelle frontal area, is expressed by

$$C_{D_N} = \left(C_{D_{\text{nacelles on}}} - C_{D_{\text{nacelles off}}}\right)\frac{S}{2S_N}$$

Preflight jet tests.- The preflight jet is of the blowdown, open-jet type and can be fitted with various nozzles for testing at supersonic and subsonic Mach numbers. A description of the preflight jet and the testing technique is given in reference 8.

The ground tests of the isolated nacelle were made using the 8-inch Mach number 1.22, 1.42, and 1.75 nozzles. Although the nacelle was large relative to the nozzle, shadowgraphs (fig. 6) show no disturbances from the nozzles entering the inlet. Since a subsonic nozzle was not available for these tests, the 8-inch Mach number 1.22 nozzle was operated at subcritical pressures and under steady-state conditions in order to determine the flow characteristics in the nacelle at a Mach number of approximately 0.8.

Pressure recovery and mass-flow ratio.- The pressure recovery and mass-flow ratios were determined by integration of the measured profiles at the test Mach numbers with the following expressions:

$$\frac{\bar{H}_d}{H_o} = \int_0^1 \frac{H_d}{H_o} d\left(\frac{y}{r}\right)^2$$

$$\frac{m}{m_o} = \frac{A_d P_d}{A_i P_o} \int_0^1 \frac{M_d}{M_o} \frac{\sqrt{1 + \frac{\gamma - 1}{2} M_d^2}}{\sqrt{1 + \frac{\gamma - 1}{2} M_o^2}} d\left(\frac{y}{r}\right)^2$$

where m_o is the mass flow through an area equivalent to the inlet area under free-stream conditions.

Accuracy.- The accuracy of drag coefficient and Mach number for the flight tests was established from tests of three identical models in reference 4. The error in pressure measurements for the flight tests and preflight tests was based on the accuaracy of the instrumentation used. A list of the errors based on the above considerations is given as follows:

C_D $(0.8 \leq M \leq 0.93$ and $1.03 \leq M \leq 1.30)$	± 0.0004
C_D $(0.93 < M < 1.03)$	± 0.001
C_{D_N} $(0.8 \leq M \leq 0.93$ and $1.03 \leq M \leq 1.30)$	± 0.05
C_{D_N} $(0.93 < M < 1.03)$	± 0.10
M_o	± 0.005
M_d	± 0.01
H_d/H_o	± 0.01
p/H_o	± 0.015
m/m_o	± 0.05

The error in C_{D_N} may be large relative to the measured values; however, values of C_{D_N} less than the drag coefficient of the isolated nacelle usually indicate the presence of favorable interference effects.

RESULTS AND DISCUSSION

Drag.- The variations of total drag coefficient with Mach number for the models tested with the inboard and wing-tip nacelles (ref. 1)

and for the basic wing-body configuration are presented in figure 7(a). The nacelle-plus-interference drag coefficients and the drag coefficients from flight tests of the isolated solid nacelle (ref. 2) are compared in figure 7(b). The internal drags of the ducted nacelles were found to be of negligible magnitude and, hence, were not subtracted from the values of C_D and C_{D_N} that are presented for the ducted nacelles. The maximum measured value of the internal-nacelle drag coefficient (based on nacelle frontal area) was only 0.02, which value is less than the experimental accuracy of the test measurements. The external drag of the isolated ducted nacelle was not obtained from the ground tests, but was estimated from reference 9 to be slightly less than that of the isolated solid nacelle between Mach numbers of 0.8 and 1.15 and somewhat greater above $M = 1.15$ for the mass-flow ratios given in figure 8.

When the solid or ducted nacelles were installed at the wing root, there was a large increase in the total drag of the configuration above a Mach number of 0.93 (fig. 7(a)). The total drag from the solid nacelle was slightly less than that from the ducted nacelle at Mach numbers greater than 1.0 and somewhat higher between Mach numbers 0.94 and 1.0. A comparison of the drags from these nacelles with that from the isolated nacelle in figure 7(b) shows that large unfavorable interference effects were obtained from both inboard nacelles near Mach number 1.0. The nacelle drags above $M = 1.05$ were approximately equal to the drag of the isolated solid nacelle. No unfavorable interference effects were obtained from either the solid or ducted nacelles below Mach number 0.93.

The comparison of nacelle drags presented in figure 7(b) for the nacelles tested at the wing root and at the wing tip (ref. 1) shows that large changes in interference effects may be obtained by changing the nacelle location, especially near Mach number 1.0. A similar observation was made in reference 2, which also showed that a transonic area rule may be used to predict the effect of nacelle location on the nacelle-plus-interference drag rise through the speed of sound. The transonic area rule, which was first presented in reference 10, states simply that the drag rise near the speed of sound is mainly dependent on the rate of development of cross-sectional area of the configuration. To aid in the application of this concept, the cross-sectional areas of the wing-body-nacelle combinations tested in this investigation and in reference 1 are given in figure 3. The amount of area subtracted from the ducted nacelles in figure 3 to compensate for the internal flow is equal to the stream tube area at the mass-flow ratio measured (fig. 8) at Mach number 1.0.

It is evident from figure 3 that the models with the inboard nacelles have a more rapid rate of development of cross-sectional area and a greater maximum cross-sectional area than the models with the wing-tip nacelles. Then, according to the transonic area rule, it would be

expected that the nacelle drag rise should be reduced by moving the nacelle from the wing root to the wing tip. This effect was obtained and is shown in figure 7(b). The unfavorable interference drag from the inboard nacelles was eliminated and favorable interference effects were obtained near Mach number 1.0 by moving the nacelles to the wing tips. The wing-tip nacelles experienced no drag rise at transonic speeds and had significantly lower drag, due to favorable interference, than the inboard nacelles at supersonic speeds. This reduction of nacelle drag may be due to either less nacelle-fuselage interference at the wing tips than at the inboard position or a favorable end-plate effect from the wing-tip nacelles or both.

At the beginning of this investigation, the inboard nacelle of reference 3 was moved from the 18-percent to the 15-percent semispan station in order to obtain the flow characteristics of the inlet located very near the fuselage. This slight movement of the nacelle made the nacelle intersect the fuselage and resulted in a slight decrease in cross-sectional area development of the configuration, but caused a large increase in drag near Mach number 1.0, indicating a limitation to the transonic area rule. The increase in drag evidently was due to unfavorable interference that resulted from the acute intersections between the fuselage and nacelle.

The drag-rise Mach number of the configuration with the inboard nacelles was 0.93, which was about 0.03 Mach number lower than that for the configuration with and without the wing-tip nacelles.

Pressure recovery.- The aerodynamic properties of the inlet of the inboard nacelle are presented in figure 9. This inlet was located very near the fuselage, with a gap between the lip and fuselage surface of only 0.35 inch. The size of the gap, however, was determined from considerations of the boundary-layer thickness that might be present on the fuselage near the inlet. The boundary-layer thickness was estimated, from flight-test data of a parabolic body of revolution presented in reference 11, to be about 0.28 inch at $M_0 = 1.25$. The gap was made only 25 percent greater than this thickness on the premise that any boundary-layer buildup behind the bow wave (normal shock) from the inlet would not exceed the size of the gap and interfere with the flow into the inlet.

A comparison of the total-pressure profiles after the diffuser of the inlet for the inboard nacelle and the isolated nacelle in figures 9(a) and 9(b) shows that both nacelles had flat total-pressure profiles of approximately the same magnitude at corresponding Mach numbers. It is evident from this comparison that the boundary layer on the fuselage near the nacelle inlet did not enter the inlet of the inboard nacelle to disturb the internal flow.

[redacted]

The variations of pressure recovery $\bar{H}_d/H_0$ with Mach number from the flight tests of the inboard nacelle and wing-tip nacelle (ref. 1) and from the ground tests of the isolated nacelle are given in figure 9(c). Good agreement was obtained between the pressure recoveries of the nacelles at corresponding Mach numbers, indicating that the wing and fuselage had a negligible effect on the pressure recovery of the nose inlet throughout the flight-test range. The total pressures measured after diffusion were about 98 percent of the free-stream total pressure at an average mass-flow ratio of 0.7 at Mach numbers from 0.8 to 1.3. The inlet pressure recovery as determined from the ground tests was only 3.5 percent less than the recovery from a normal shock at Mach number 1.75 (fig. 9(c)) and a mass-flow ratio of 0.96.

Figure 9(d) shows the variations of static pressure at the diffuser measuring station from $M_0 = 0.8$ to 1.75 as determined by the flight and ground tests.

CONCLUSIONS

The results of flight tests between Mach numbers of 0.8 to 1.3 of a 45° sweptback-wing—body configuration with nacelles (having NACA 1-50-250 nose inlets) located at the wing roots and comparisons with the results of previous tests of wing-tip nacelles and isolated nacelles are as follows:

1. The nacelle-plus-interference drag rise from the nacelles was in general dependent on the nacelle location and in part dependent on the resulting rate of development of cross-sectional area of the aircraft configuration.

2. Little or no unfavorable interference effects were obtained from either the solid or ducted inboard nacelles above Mach number 1.05 and below Mach number 0.93, whereas, favorable interference was obtained from the wing-tip nacelles throughout the flight range.

3. The wing and body had a negligible effect on the total-pressure recovery of the inlet diffuser in either the inboard or wing-tip nacelle positions. The total pressure after diffusion was about 98 percent of the free-stream total pressure at a mass-flow ratio of about 0.7 throughout the flight-test range.

4. The drag-rise Mach number of the configuration with the inboard nacelles was 0.93, which was about 0.03 Mach number lower than that for the configuration with and without the wing-tip nacelles.

Langley Aeronautical Laboratory,
National Advisory Committee for Aeronautics,
Langley Field, Va., August 10, 1953.

[redacted]

REFERENCES

1. Hoffman, Sherwood, and Pepper, William B., Jr.: Transonic Flight Tests To Determine Zero-Lift Drag and Pressure Recovery of Nacelles Located at the Wing Tips on a 45° Sweptback Wing and Body Combination. NACA RM L51K02, 1952.

2. Hoffman, Sherwood, and Pepper, William B., Jr.: The Effect of Nacelle Combinations and Size on the Zero-Lift Drag of a 45° Sweptback Wing and Body Configuration as Determined by Free-Flight Tests at Mach Numbers Between 0.8 and 1.3. NACA RM L53E25, 1953.

3. Pepper, William B., Jr., and Hoffman, Sherwood: Comparison of Zero-Lift Drags Determined by Flight Tests at Transonic Speeds of Symmetrically Mounted Nacelles in Various Spanwise Positions on a 45° Sweptback Wing and Body Combination. NACA RM L51D06, 1951.

4. Pepper, William B., Jr., and Hoffman, Sherwood: Transonic Flight Tests To Compare the Zero-Lift Drag of Underslung and Symmetrical Nacelles Varied Chordwise at 40 Percent Semispan of a 45° Sweptback, Tapered Wing. NACA RM L50G17a, 1950.

5. Hoffman, Sherwood: Transonic Flight Tests To Compare the Zero-Lift Drags of Underslung Nacelles Varied Spanwise on a 45° Sweptback Wing and Body Combination. NACA RM L52D04a, 1952.

6. Pepper, William B., Jr., and Hoffman, Sherwood: Comparison of Zero-Lift Drags Determined by Flight Tests at Transonic Speeds of Symmetrically Mounted Nacelles in Various Chordwise Positions at the Wing Tip of a 45° Sweptback Wing and Body Combination. NACA RM L51F13, 1951.

7. Hoffman, Sherwood, and Mapp, Richard C., Jr.: Transonic Flight Tests To Compare the Zero-Lift Drags of 45° Sweptback Wings of Aspect Ratio 3.55 and 6.0 With and Without Nacelles at the Wing Tips. NACA RM L51L27, 1952.

8. Faget, Maxime A., Watson, Raymond S., and Bartlett, Walter A., Jr.: Free-Jet Tests of a 6.5-Inch-Diameter Ram-Jet Engine at Mach Numbers of 1.81 and 2.00. NACA RM L50L06, 1951.

9. Sears, Richard I., and Merlet, C. F.: Flight Determination of the Drag and Pressure Recovery of an NACA 1-40-250 Nose Inlet at Mach Numbers From 0.9 to 1.8. NACA RM L50L18, 1951.

10. Whitcomb, Richard T.: A Study of the Zero-Lift Drag-Rise Characteristics of Wing-Body Combinations Near the Speed of Sound. NACA RM L52H08, 1952.

11. Rumsey, Charles B., and Loposer, J. Dan: Average Skin-Friction Coefficients From Boundary-Layer Measurements in Flight on a Parabolic Body of Revolution (NACA RM-10) at Supersonic Speeds and at Large Reynolds Numbers. NACA RM L51B12, 1951.

[redacted]

TABLE I

FUSELAGE COORDINATES

x, in.	y, in.
0	0
.4	.185
.6	.238
1.0	.342
2.0	.578
4.0	.964
6.0	1.290
8.0	1.577
12.0	2.074
16.0	2.472
20.0	2.772
24.0	2.993
28.0	3.146
32.0	3.250
36.0	3.314
40.0	3.334
44.0	3.304
48.0	3.219
52.0	3.037
56.0	2.849
60.0	2.661
64.0	2.474
66.7	2.347

NACA

TABLE II

COORDINATES OF THE NACA 65A009 AIRFOIL

x/c, percent	y/c, percent
0	0
.5	.690
.75	.837
1.25	1.068
2.5	1.463
5.0	1.965
7.5	2.385
10.0	2.736
15.0	3.292
20.0	3.714
25.0	4.034
30.0	4.266
35.0	4.420
40.0	4.495
45.0	4.485
50.0	4.379
55.0	4.173
60.0	3.881
65.0	3.519
70.0	3.099
75.0	2.630
80.0	2.125
85.0	1.601
90.0	1.074
95.0	.547
100.0	.020
Leading-edge radius, 0.00516c	

NACA

[redacted]

TABLE III

COORDINATES FOR NACELLE INNERBODY

Modified airfoil section

x, in.	y, in.
0	0
.154	.316
.730	.380
1.307	.428
1.884	.465
2.461	.492
3.037	.510
3.614	.518
6.285	.504
6.848	.492
7.410	.469
7.972	.436
8.534	.395
9.097	.348
9.659	.296
10.221	.239
10.783	.180
11.346	.121
11.908	.062
12.470	.002
Leading-edge radius, 0.335 in.	

NACA

TABLE IV

COORDINATES FOR SOLID NACELLE

x, in.	y, in.
0	0
.100	.070
.330	.169
.830	.336
1.330	.489
1.830	.622
2.330	.747
2.580	.800
2.958	.876
3.585	.974
4.840	1.105
6.095	1.190
7.350	1.240
8.605	1.255
16.830	1.255
17.872	1.237
18.913	1.195
19.955	1.127
20.996	1.029
22.038	.909
23.079	.768
24.121	.616
24.250	.598

NACA

TABLE V

COORDINATES FOR DUCTED NACELLE

External		Internal	
x, in.	y, in.	x, in.	y, in.
0	0.661		
.063	.723		
.188	.770		
.251	.789		
.439	.836		
.628	.876		
1.255	.974	0	0.63
2.196	1.077	2.00	.75
3.138	1.152	3.00	.75
4.393	1.219	4.332	1.075
6.275	1.255	6.275	1.075
14.500	1.255	14.500	1.075
15.542	1.237	15.542	1.057
16.583	1.195	16.583	1.010
17.625	1.127	17.625	.955
18.666	1.029	18.666	.882
19.708	.909	19.708	.791
20.749	.768	20.749	.690
21.791	.616	21.791	.585
21.920	.598	21.920	.575
Lip radius, 0.03 in.			

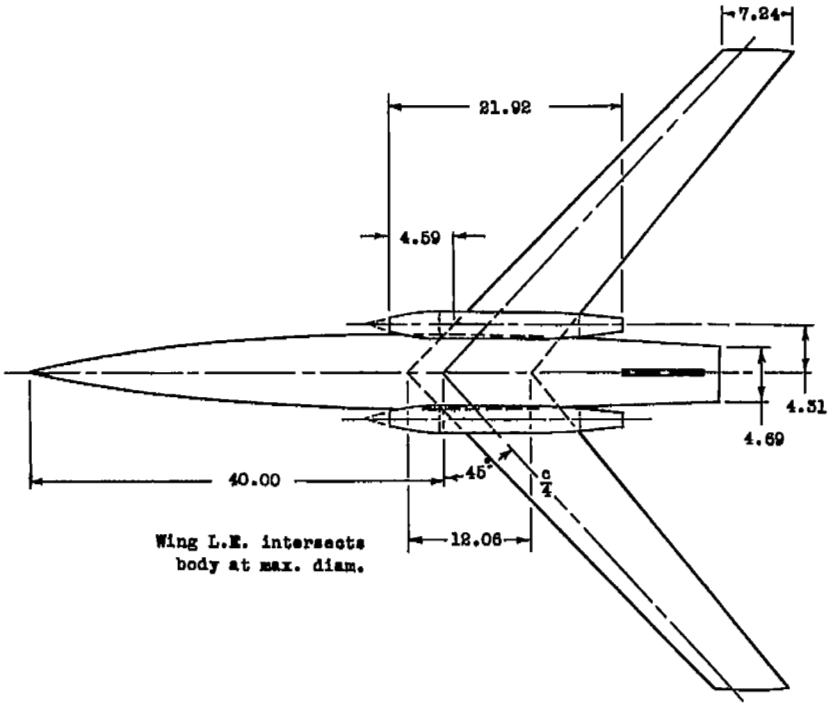

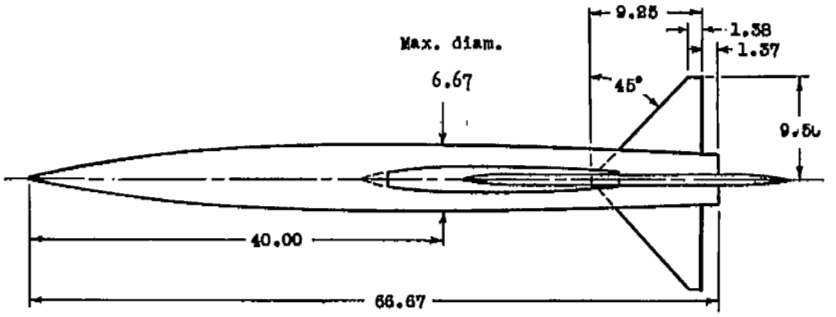

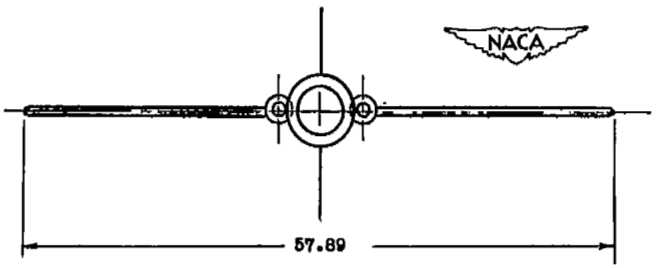

Model characteristics:

Body fineness ratio	10.0
Wing aspect ratio	6.0
Wing taper ratio	0.6
Mean aerodynamic chord, ft	0.822
Airfoil parallel to free stream	NACA 65A009
Total wing plan-form area, sq ft	3.878
Exposed wing plan-form area, sq ft	3.333
Exposed wing frontal area, sq ft	0.299
Body frontal area, sq ft	0.242
Total frontal area, sq ft	0.550
Exposed fin plan-form area (2 fins), sq ft	0.468

Fins are flat plates and 0.091 inch thick with 0.045-inch radius at edges.

Nacelle fineness ratio (ducted)	8.73
Nacelle fineness ratio (solid)	9.66
Frontal area of one nacelle, sq ft	0.034
Nose inlet of nacelle	NACA 1-50-250

Figure 1.- General arrangement and dimensions of test model. All dimensions are in inches.

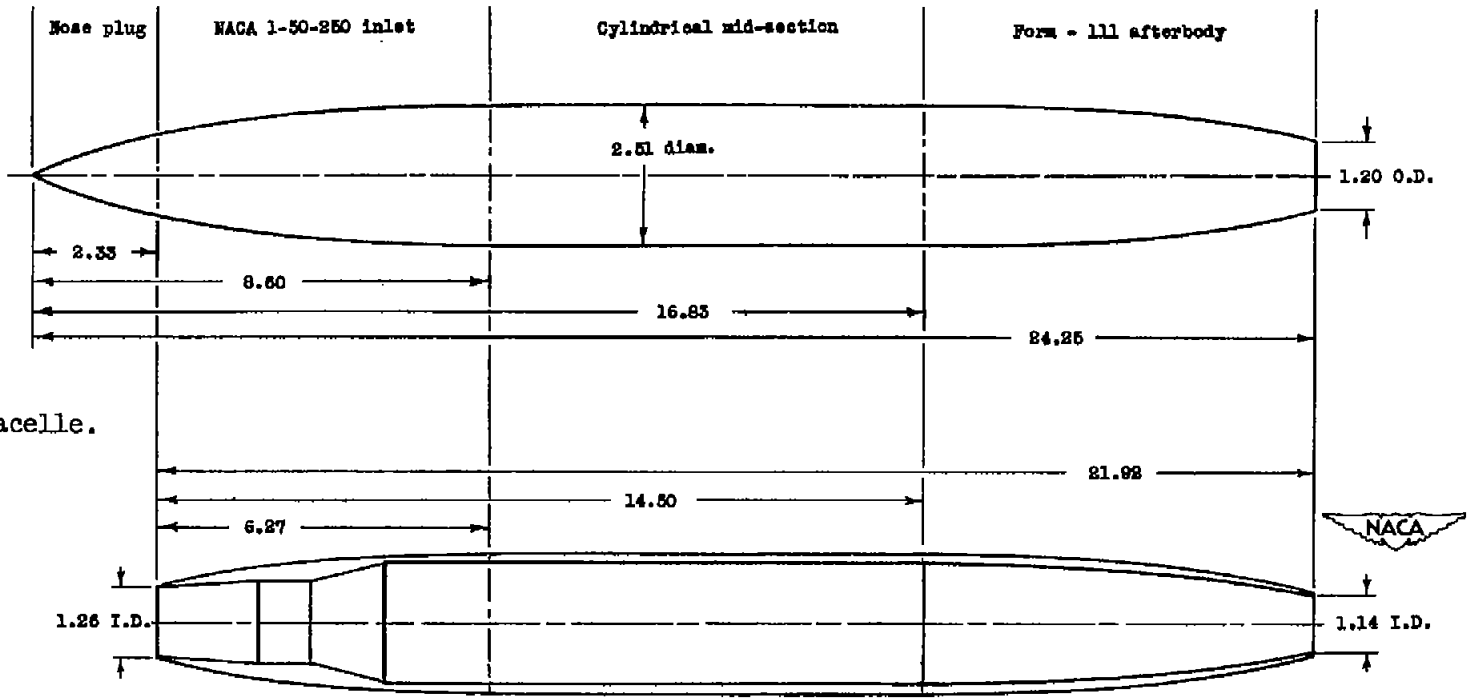

(a) Solid nacelle.

(b) Ducted nacelle.

Figure 2.- Details and dimensions of solid nacelle, ducted nacelle, and nacelle inlets used for the ground tests and flight tests. All dimensions are in inches.

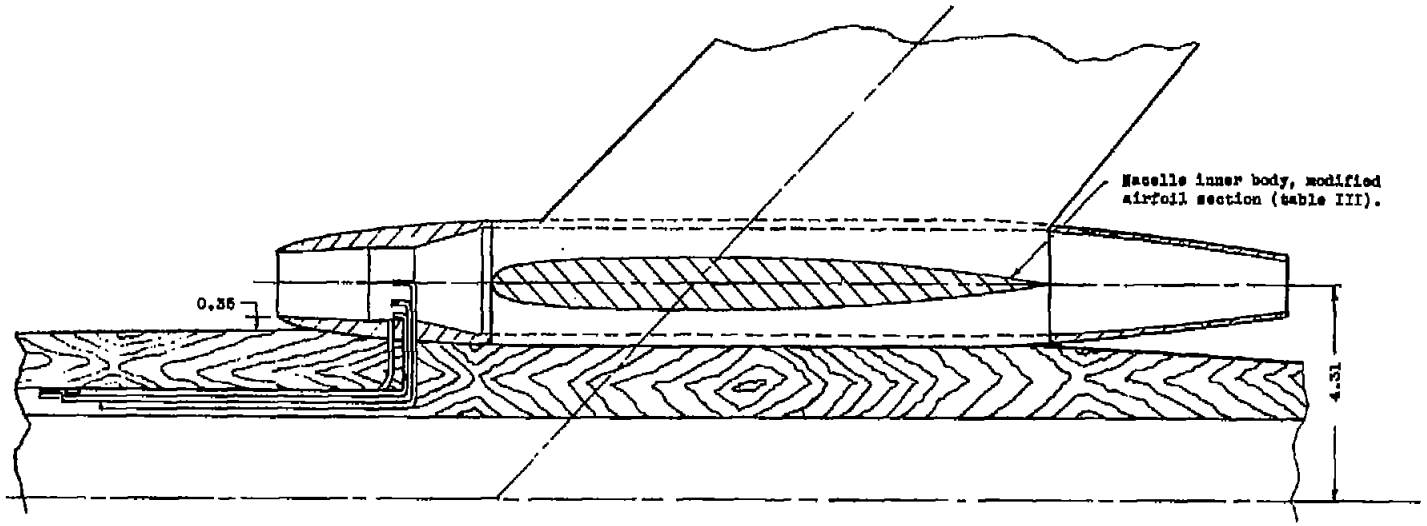

(c) Nacelle installation at wing root.

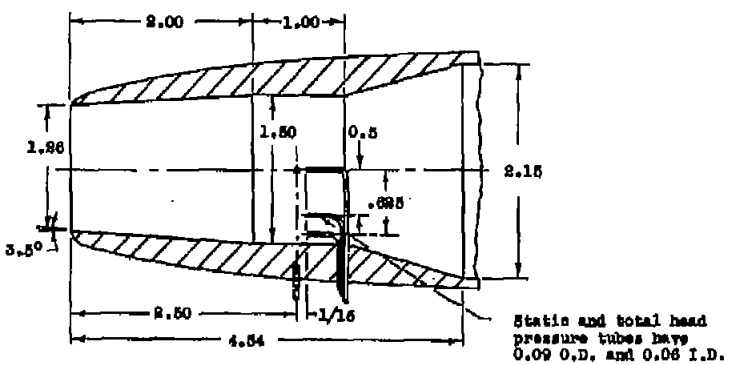

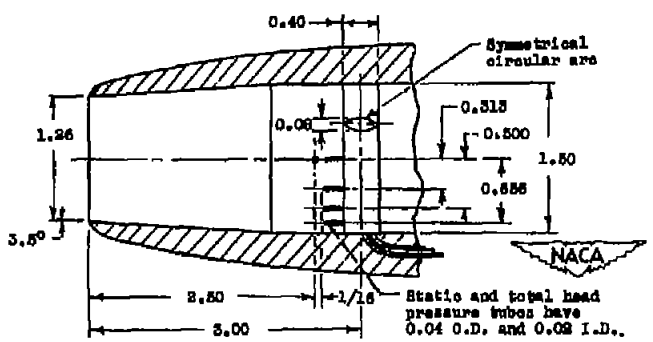

(d) Inlet for flight test. (e) Inlet for ground test.

Figure 2.- Concluded.

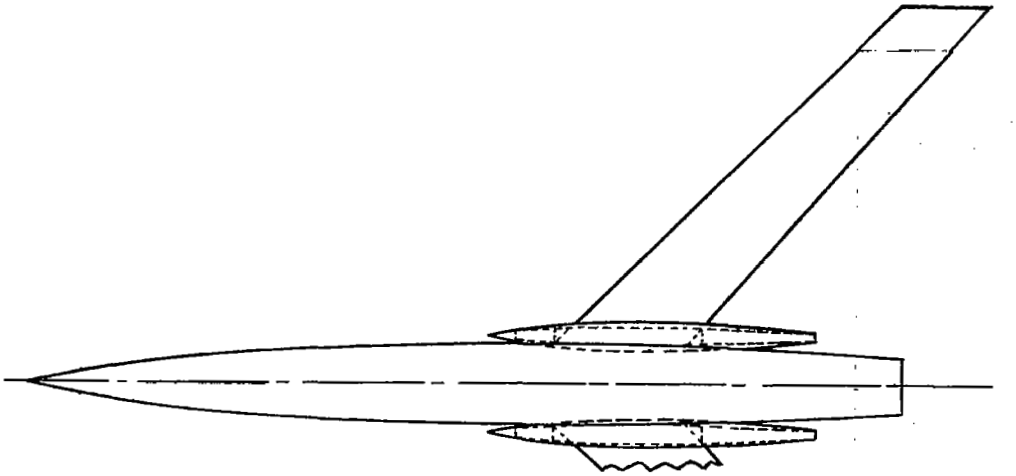

(a) Model with inboard nacelles.

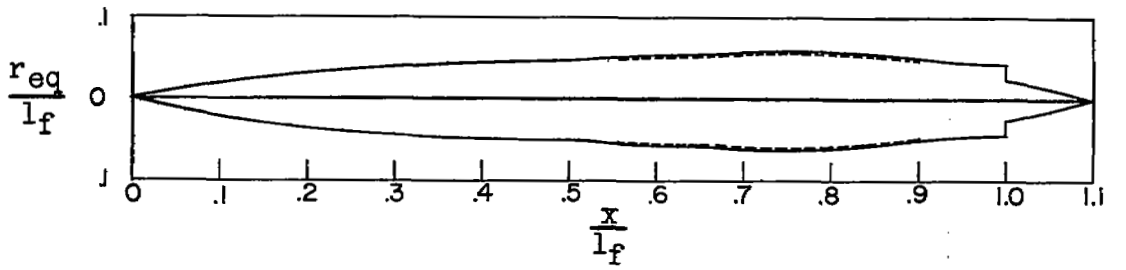

(b) Equivalent body of revolution for model with inboard nacelles.

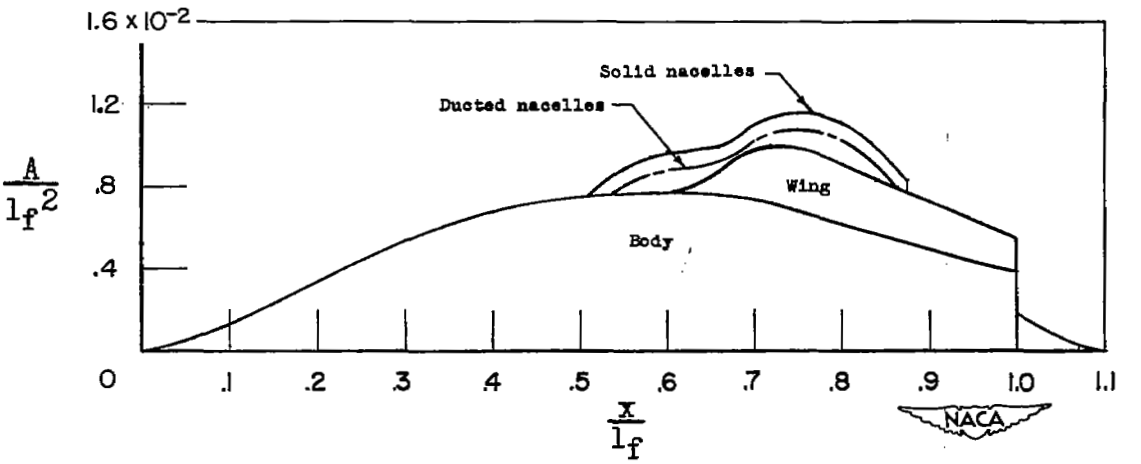

(c) Cross-sectional area distribution for model with inboard nacelles.

Figure 3.- Cross-sectional area distribution of wing-body-nacelle models.

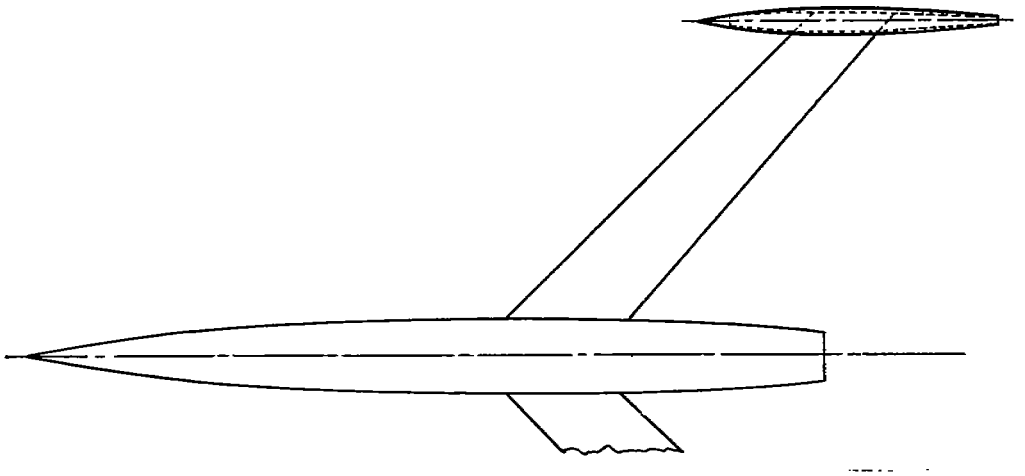

(d) Model with wing-tip nacelles.

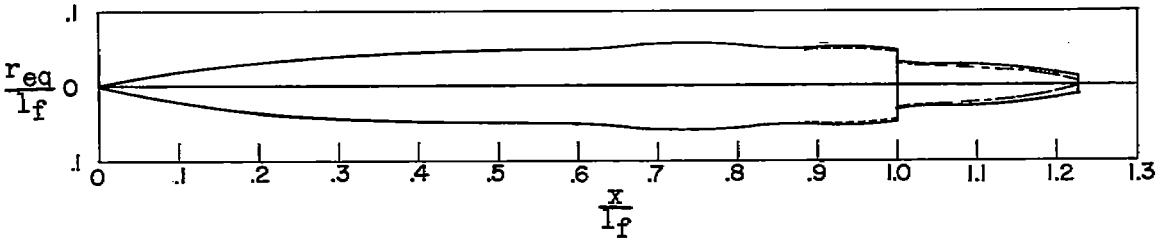

(e) Equivalent body of revolution for model with wing-tip nacelles.

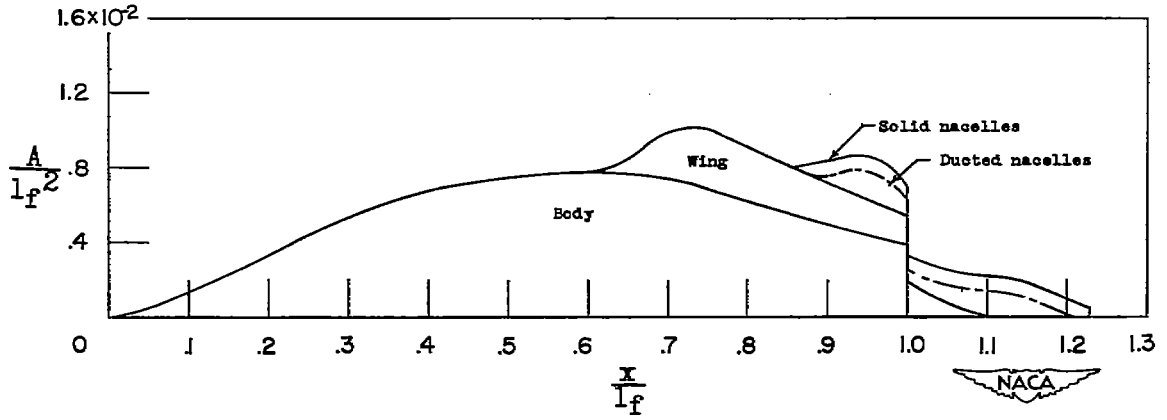

Cross-sectional area distribution for model with wing-tip nacelles (ref. 1).

Figure 3.- Concluded.

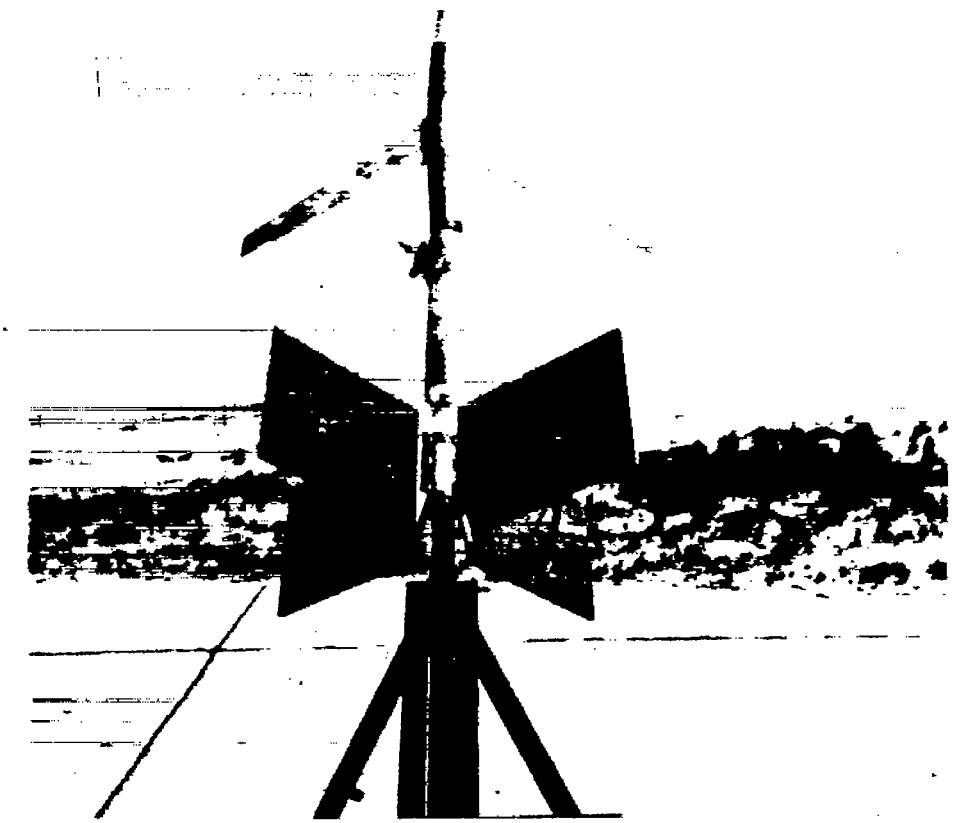

L-61049

(a) Basic configuration and booster on rail launcher.

Figure 4.- Photographs of flight models.

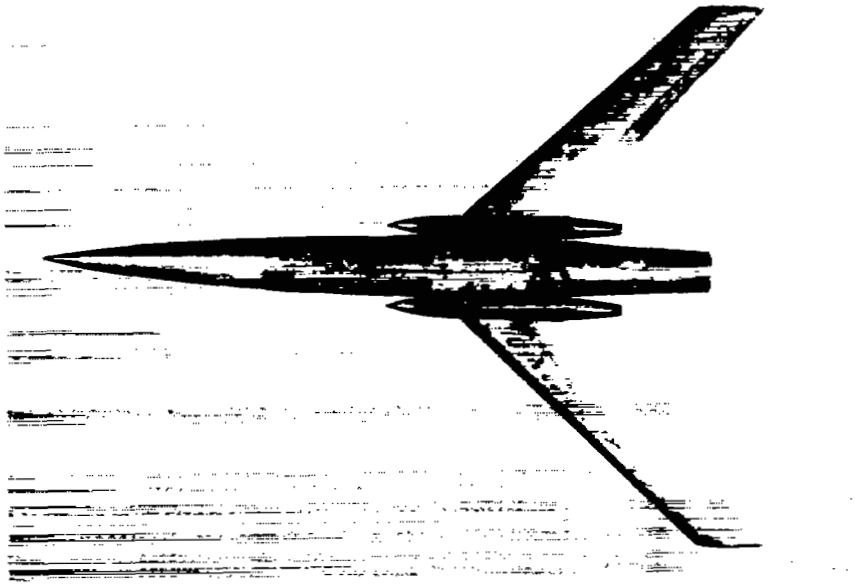

L-73580.1

(b) Model with solid nacelles at wing root.

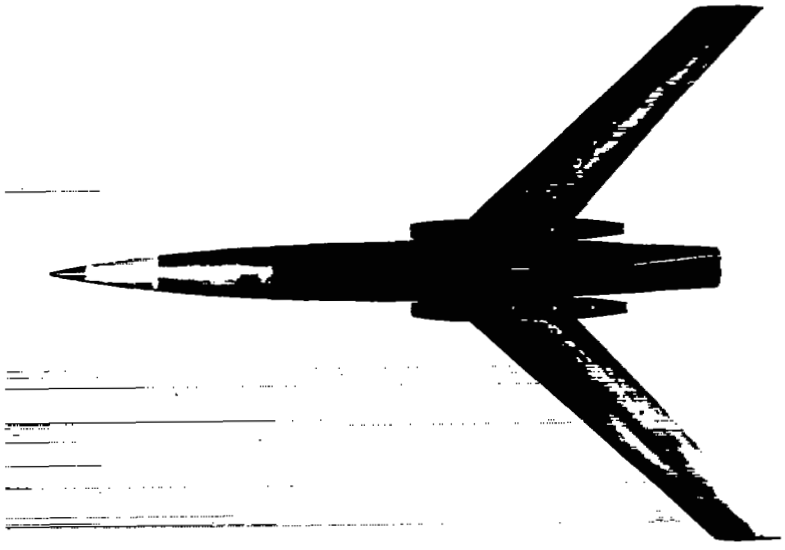

L-77142.1

(c) Model with ducted nacelles at wing root.

Figure 4.- Continued.

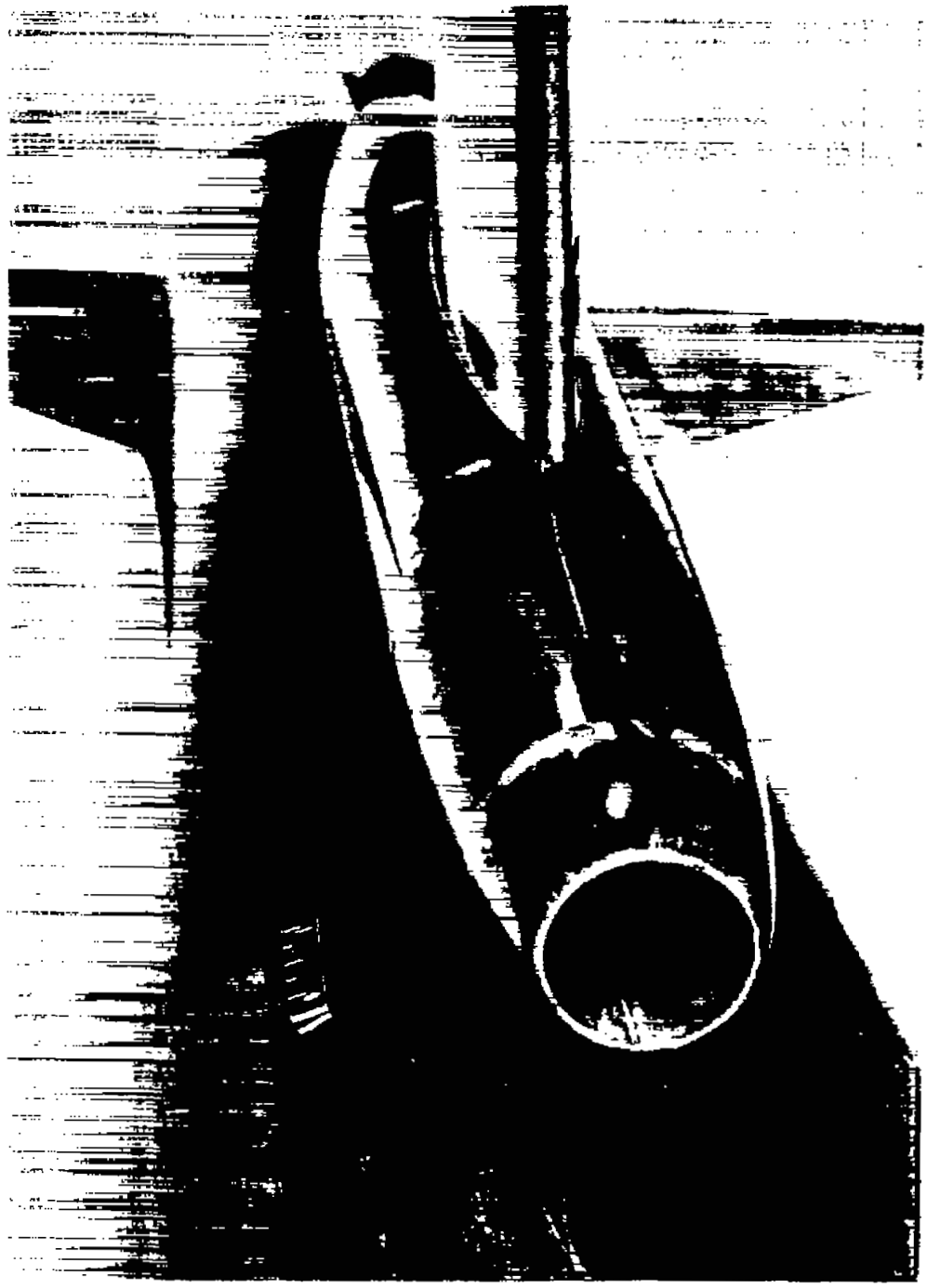

(d) View of nacelle installation at wing root. L-77144.1

Figure 4.- Continued.

T

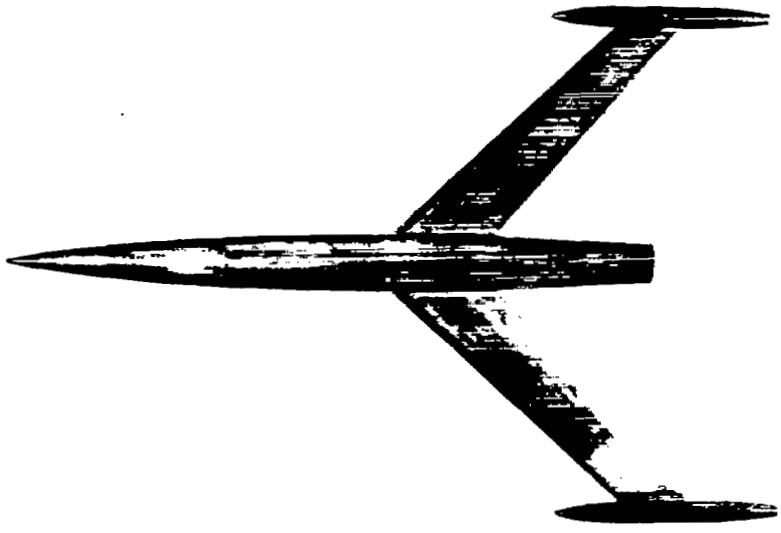

L-67573.1

(e) Model with solid nacelles at wing tips (ref. 1).

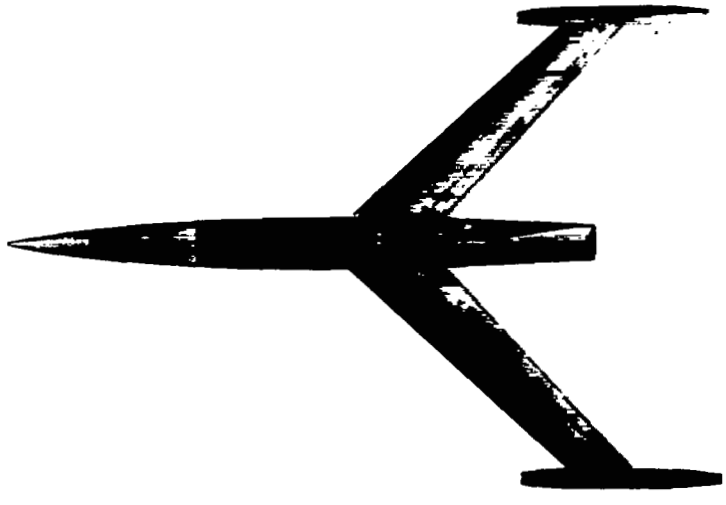

L-69938.1

(f) Model with ducted nacelles at wing tips (ref. 1).

Figure 4.- Concluded.

[redacted]

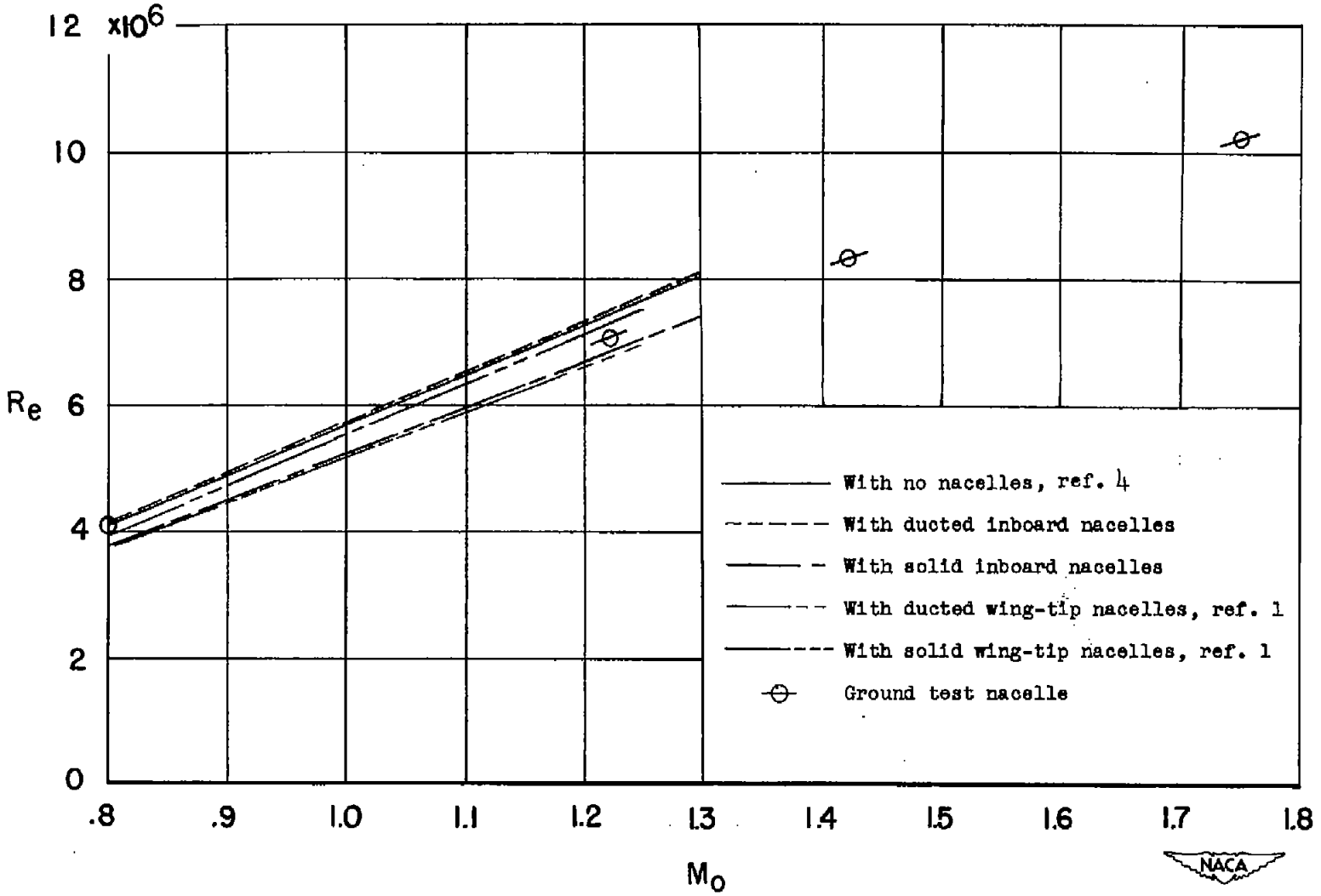

Figure 5.- Variation of Reynolds number with Mach number for models tested. (Reynolds number based on wing mean aerodynamic chord.)

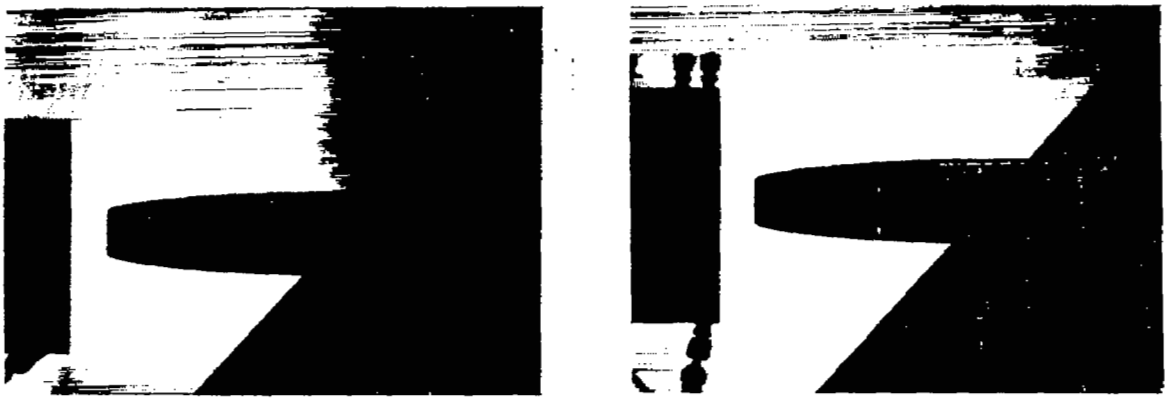

(a) M_o = 1.22. (b) M_o = 1.42.

(c) M_o = 1.75. L-70845

Figure 6.- Shadowgraphs of NACA 1-50-250 nose inlet in preflight jet.

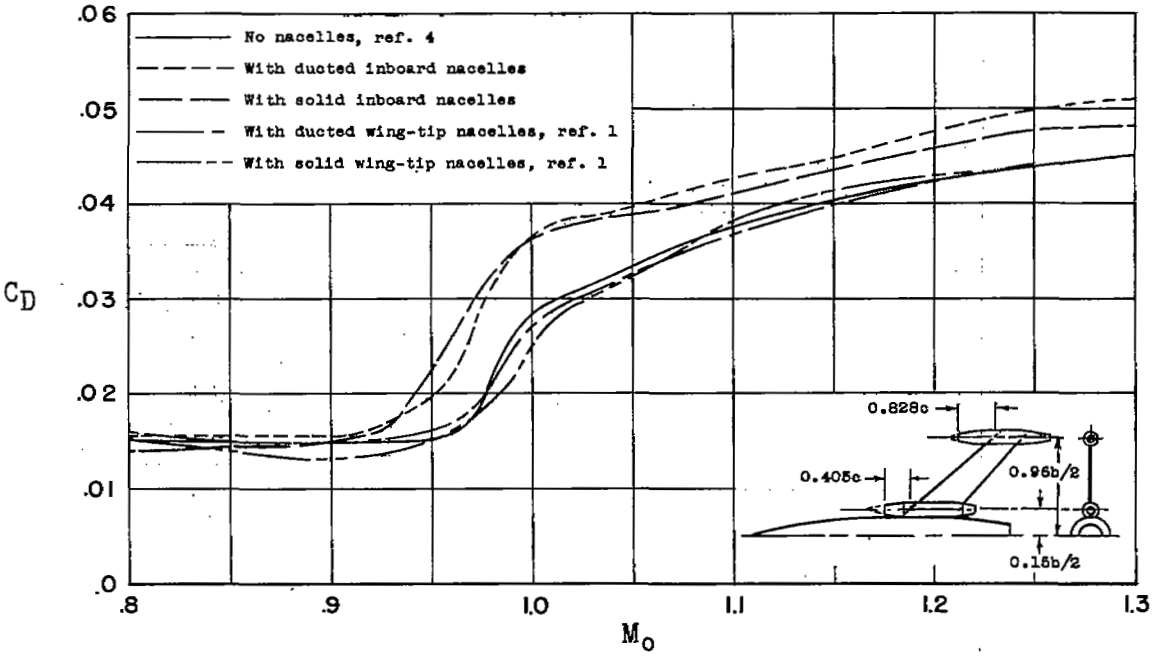

(a) Variations of total-drag coefficients with Mach number.

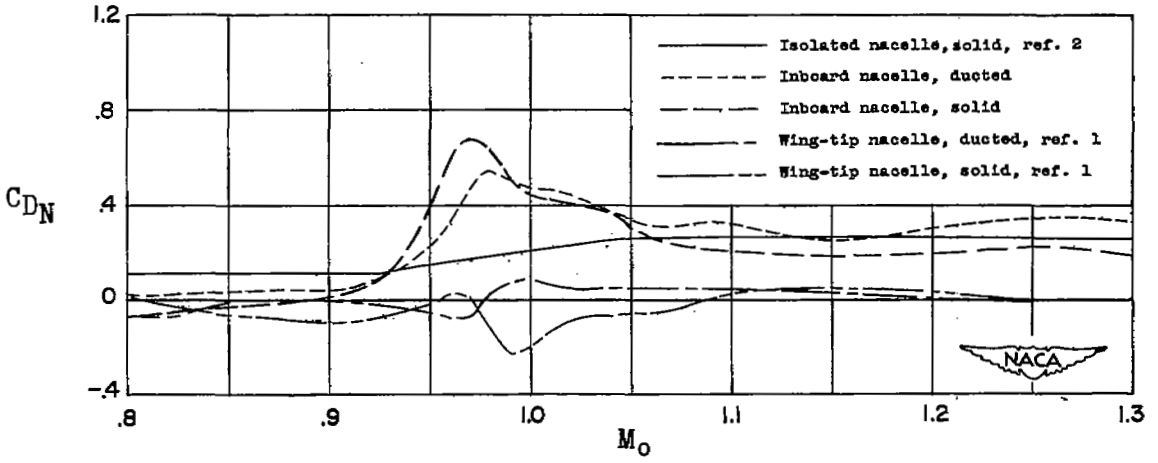

(b) Variations of nacelle-plus-interference drag coefficients with Mach number.

Figure 7.- Variations of total-drag coefficients and nacelle-plus-interference drag coefficients with Mach number for models tested.

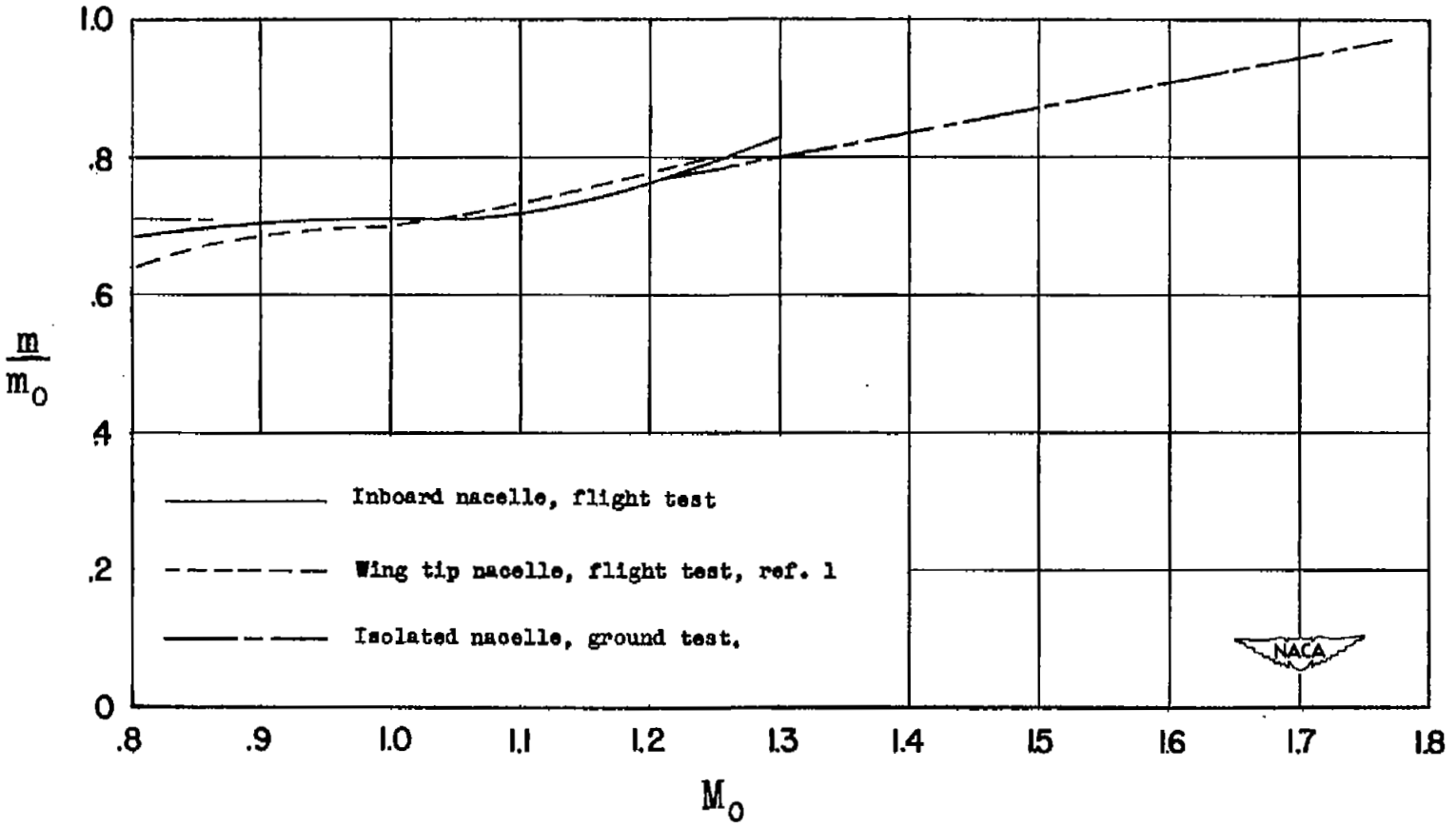

Figure 8.- Variation of mass-flow ratio with Mach number.

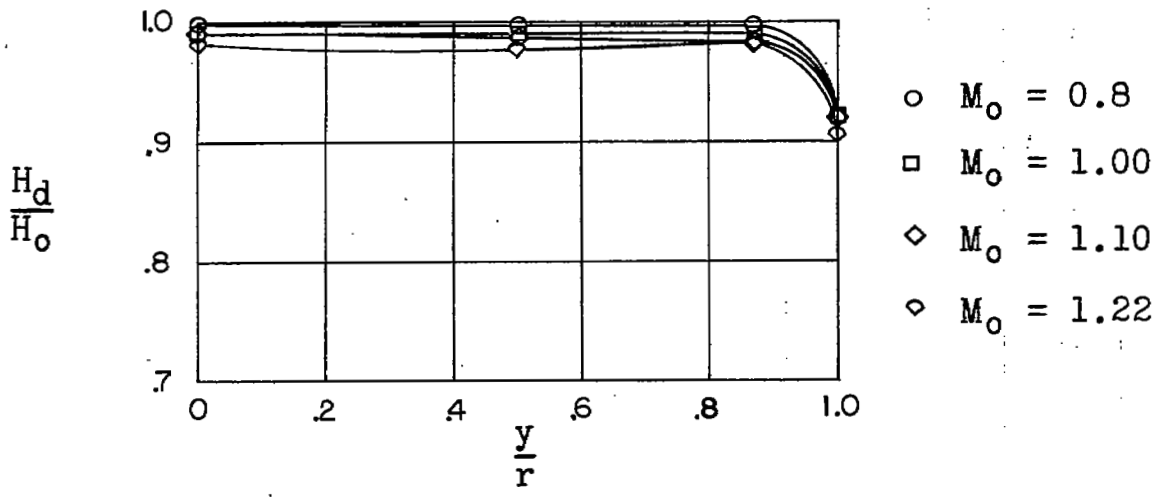

(a) Total-pressure profile after diffuser for several Mach numbers as determined by flight test of inboard nacelles.

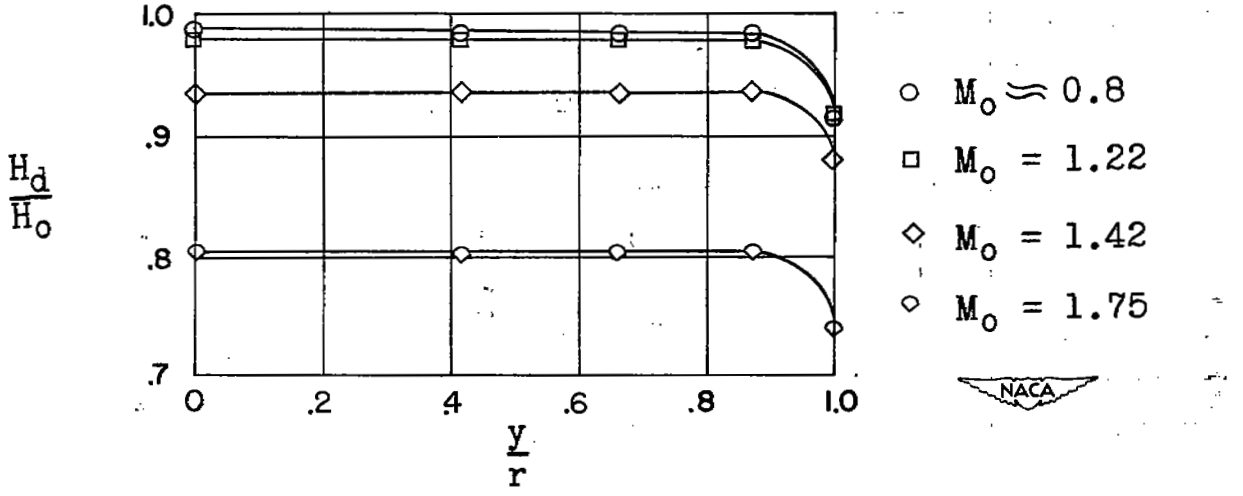

(b) Total-pressure profile after diffuser for several Mach numbers as determined by ground tests of the isolated nacelle.

Figure 9.- Properties of ducted nacelle with an NACA 1-50-250 inlet as determined by flight tests and ground tests.

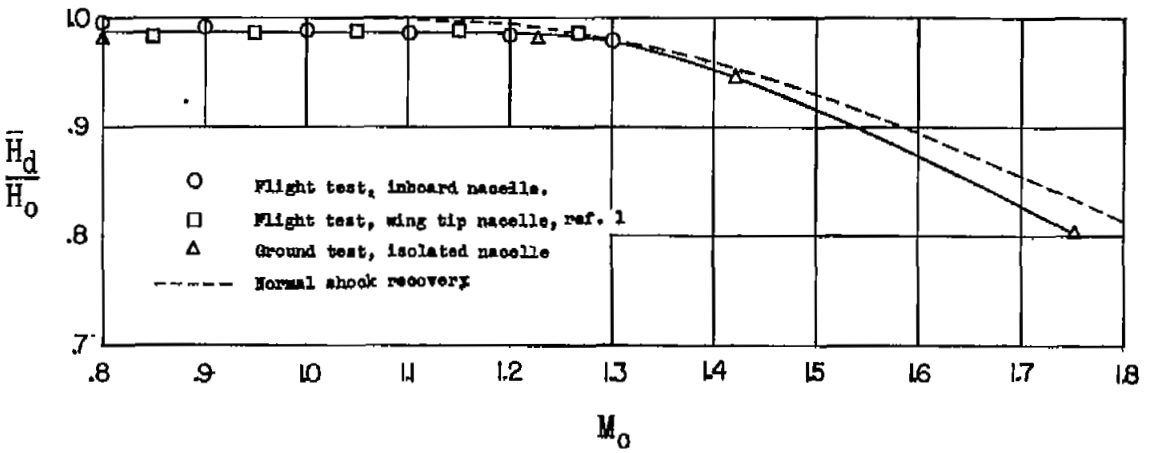

(c) Variation of diffuser pressure recovery with Mach number.

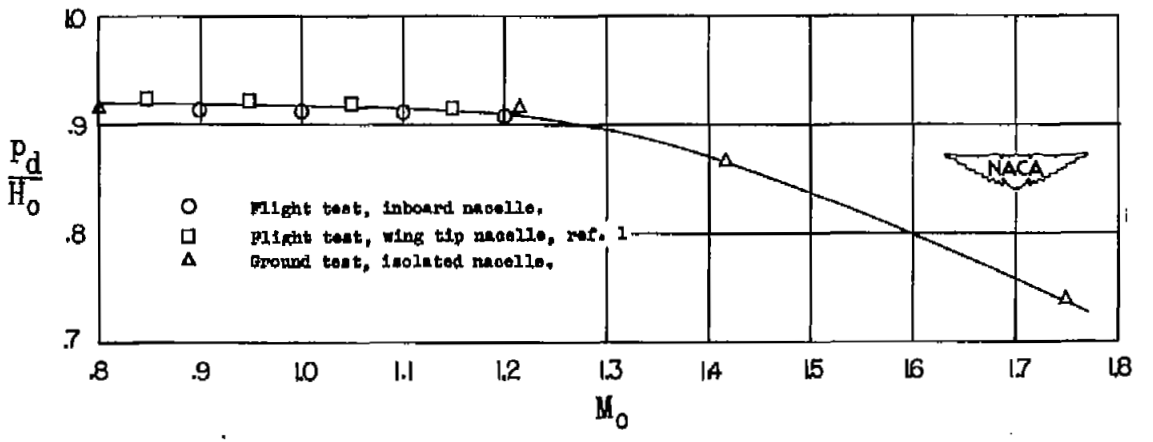

(d) Variation of static pressure after diffuser with Mach number.

Figure 9.- Concluded.

[redacted]